Distribution and Lateral Mobility of Voltage-dependent Sodium Channels in Neurons

Kimon J. Angelides, Lawrence W. Elmer, David Loftus,* and Elliot Elson*

Department of Physiology and Molecular Biophysics, Baylor College of Medicine, Houston, Texas 77030; and *Department of Biological Chemistry, Washington University School of Medicine, St. Louis, Missouri 63110

Abstract. Voltage-dependent sodium channels are distributed nonuniformly over the surface of nerve cells and are localized to morphologically distinct regions. Fluorescent neurotoxin probes specific for the voltage-dependent sodium channel stain the axon hillock 5–10 times more intensely than the cell body and show punctate fluorescence confined to the axon hillock which can be compared with the more diffuse and uniform labeling in the cell body. Using fluorescence photobleaching recovery (FPR) we measured the lateral mobility of voltage-dependent sodium channels over specific regions of the neuron. Nearly all sodium channels labeled with specific neurotoxins are free to diffuse within the cell body with lateral diffusion coefficients on the order of 10^{-9} cm^2/s. In contrast, lateral diffusion of sodium channels in the axon hillock is restricted, apparently in two different ways. Not only do sodium channels in these regions diffuse more slowly (10^{-10}-10^{-11} cm^2/s), but also they are prevented from diffusing between axon hillock and cell body. No regionalization or differential mobilities were observed, however, for either tetramethylrhodamine-phosphatidylethanolamine, a probe of lipid diffusion, or FITC-succinyl concanavalin A, a probe for glycoproteins. During the maturation of the neuron, the plasma membrane differentiates and segregates voltage-dependent sodium channels into local compartments and maintains this localization perhaps either by direct cytoskeletal attachments or by a selective barrier to channel diffusion.

THE segregation or clustering of surface components into discrete and functionally significant domains is an important feature of neuronal cell biology. Obvious examples are the structure of the synapse and its postsynaptic configuration containing a high density of transmitter receptors, and the segregation of various other components to dendrites, cell bodies, axons, or even local domains within these areas. Two specific systems that have been used to investigate the mechanisms underlying the processes of segregation are the neuromuscular junction, where acetylcholine receptors are clustered on the postsynaptic muscle fiber (25), and the node of Ranvier in myelinated axons to which voltage-dependent sodium channels are segregated (43).

Propagation of the action potential in nerve depends on the presence of voltage-sensitive sodium and potassium channels, and it has long been recognized that in myelinated fibers the nodes of Ranvier are the sites of large inward sodium currents that mediate the saltatory conduction of the action potential. Since the sodium channel system lends such unique excitability characteristics to the cell membrane (15), there is great interest in localizing and quantifying sodium channels at specific sites on the cell. This distribution of channels will determine some of the differential electrical properties of one part versus another part of a given excitable cell. A number of laboratories have recently isolated and characterized the sodium channel protein as an extremely carbohydrate-rich polypeptide of M_r 260 kD (9, 22, 26, 36). Although localization of important receptors and some morphological and electrophysiological evidence on sodium channel distribution has been described (4–6, 17, 20, 43, 57), little is known concerning the mechanisms that regulate and maintain their surface localization. Biological membranes can be considered to be two-dimensional fluids. Many membrane proteins that are dispersed in this medium have been shown to be mobile in the membrane plane (13). This mobility is physiologically important in some instances (8). Selected examples are the diffusion mediated aggregation of some peptide hormone receptors into microclusters as a prelude to endocytosis and the metabolically driven collection of cell surface receptors into a cap when lymphocytes are exposed to multivalent ligands such as antibodies and lectins (8, 24). However, unlike the above phenomena, the maintenance of polarity in a neuron requires that the membrane be organized over long distances.

Neurons offer a particularly important system in which to investigate the functional consequences of the distribution and mobility of cell surface components. The highly assymmetric nature of nerve cells and lack of protein synthetic machinery at the distal end requires that many cell surface components be organized and transported great distances. These proteins may be axonally transported and inserted locally, or they may reach their destination by lateral diffusion through

the plasma membrane after insertion into the soma. A recent study of intramembrane particle (IMP)[1] redistribution, correlated with the appearance of [^{3}H]Saxitoxin binding, has suggested a surface transport mechanism for processing sodium channels in growing axons. In this case the rate of transport of the particles (sodium channels) along the surface of the axon was limited not by diffusion but by the extension and the addition of new membrane at the growth cone of the advancing neurite (49, 50, 52).

The mobility of sodium channels, the mechanisms by which they are distributed over neurons, and the maintenance of this distribution are important issues for the physiology of excitable cells.

To understand the cellular mechanisms and factors during neuronal differentiation and development that initiate compartmentalization, and those cellular structures that maintain this regionalization, we have measured the lateral mobility of sodium channels in isolated mature neurons maintained in culture. This study is prerequisite to examining those cellular influences contributed by either ensheathing cells (e.g., Schwann cells) or by target tissue (muscle). Using a number of fluorescent probes specific for the voltage-dependent sodium channel, we have used fluorescence photobleaching recovery (FPR) to measure the lateral diffusion of sodium channels at specific regions of mature rat cortical and spinal cord neurons grown in culture. We have shown that voltage-dependent sodium channels are sparsely distributed and freely mobile on the nerve cell body while they are densely distributed and relatively immobile at the axon hillock and neuritic terminal.

Materials and Methods

Fluorescent Sodium Channel Probes

Biologically active fluorescent α-scorpion toxins (3-(7-nitroben-2-oxa-1,3-diazol-4-yl-toxin V from the venom of *Leiurus quinquestriatus quinquestriatus* [NBD-Lqq V] and 7-diethylaminocoumarin-4-phenylmaleimido-thio-Lqq V [CPM-Lqq V]), β-scorpion toxin derivatives (CPM-thio-toxin from *Centruroides suffussus suffussus* [CPM-Css II]), and tetrodotoxin (NBD-TTX [NBD-tetrododotoxin]) were prepared as previously described (1, 3, 6, 17). TmRhd-Lqq V (6-carboxytetramethyl rhodamine acetamide-Lqq V) and TmRhd-Tityus γ (a β-scorpion toxin) were prepared according to previously published procedures by selective acylation of Lys 60 of Lqq V or Lys 13 of Tityus γ with the succinimidyl ester of 5(6)carboxytetramethylrhodamine (3). Equilibrium binding to rat brain synaptosomes, to cultured cortical, or spinal cord neurons show that the K_d for TmRhd-Lqq V binding is 7, 7, and 6.5 nM, respectively. Intracellular recording of muscle action potentials shows that the derivative is biologically effective with a $K_{0.5}$ of 4 nM in prolonging the falling phase of the action potential. TmRhd-Tityus γ is also biologically active in blocking spinal cord neuron single sodium channel currents in cell-attached patches; the effective $K_{0.5}$ is ~4 nM.

TmRhd-phosphatidylethanolamine (TmRhd-PE) was obtained from Avanti Polar Lipids Inc. (Birmingham, AL). 1,1'-dioctadecyl-3,3,3',3'-tetrametramethylindocarbocyanine (DiI) was obtained from Molecular Probes, Inc. (Junction City, OR). Affinity-purified rabbit IgG raised against each of the neurofilament proteins (NF1, NF2, and NF3) were produced in this laboratory by Kirk Smith and characterized as described (35). Rabbit anti-glial fibrillary acidic protein was purchased from Accurate Chemical & Scientific Corp. (Westbury, NY).

1. *Abbreviations used in this paper*: CPM, 7-diethylaminocoumarin-4-phenylmaleimido-thio; Css II, toxin II from *Centruroides suffussus suffussus*; FPR, fluorescence photobleaching recovery; IMP, intramembrane particle; Lqq V, toxin V from the venom of *Leiurus quinquestriatus quinquestriatus*; NBD, 7-nitrobenz-2-oxa-1,3 diazol; PE, phosphatidylethanolamine; TmRhd, 6-carboxytetramethyl rhodamineacetamide; TTX, tetrodotoxin; WGA, wheat germ agglutinin.

Preparation and Labeling of Cells

Two neuronal culture systems were used for the FPR studies. Dissociated rat embryonic cortical neurons were cultured on 0.13-mm-thick polylysine-coated glass coverslips in 35-mm Petri dishes and maintained in 5% FCS and 10% horse serum in DME. Growth of nonneuronal cells was eliminated by adding 5-fluoro-2'-deoxyuridine and cytosine arabinoside to the cultures. Rat embryonic spinal cord cell cultures were prepared using the method of Ransom et al. (42), and plated on 0.13-mm-thick glass coverslips coated with polylysine. Cells were maintained in a medium of CO_2-equilibrated DME (7% CO_2) with 10% fetal calf serum and 10% horse serum. Cells were maintained in this medium until the background cells formed a confluent monolayer. After 2 d, the medium was changed to DME with 10% horse serum plus 35 μg/ml of uridine and 15 μg/ml 5'-fluoro-2'-deoxyuridine to kill dividing nonneuronal cells. After 2 d the medium was changed to DME with 10% horse serum for the remainder of the growth period. Approximately 5% of the cells in the culture were glia as assessed immunocytochemically with antibodies specific for glial fibrillary acidic protein.

Spinal cord cell cultures were used for study as they have the largest number of well isolated neurons. Cultures were studied after 2–6 wk of development in vitro at which time functional synaptic connections measured electrophysiologically (28, 42), the maturation of neurons, and the densities of sodium channels assessed by neurotoxin binding, were at a maximum. The stage of neuronal growth was determined by immunocytochemistry for the appearance and locale of each of the neurofilament proteins. These proteins provide the best markers for neuronal differentiation (since nonneuronal cells do not contain this class of intermediate filaments) and also serve to define the developmental stage and maturation of the neuron (47, 48).

Labeling

The α- and β-scorpion toxins bind to a single class of receptor sites on the sodium channel of excitable cells with K_ds between 2 and 8 nM (1, 3, 17). The half-time for dissociation is about 65 min at 22°C for NBD-Lqq V, TmRhd-Lqq V, and CPM-Css II, 5 min for NBD-TTX, and ~3 h for TmRhd-Tityus γ. Before photobleaching experiments, confluent cultures, grown under standard conditions, were incubated with 10 nM fluorescent Lqq V, Css II, Tityus γ, or TTX for 30 min at room temperature in standard binding medium consisting of 130 mM choline chloride, 5.4 mM KCl, 0.8 mM $MgSO_4$, 5.5 mM glucose, and 50 mM Hepes adjusted to pH 7.4 with Tris base. The cultures were then rapidly washed three times with ice-cold standard binding buffer or ice-cold PBS. In some experiments the fluorescent scorpion toxins were incubated in PBS, which included 2 μM TTX to block ion movement through the channels which would lead to membrane depolarization. Since the binding of NBD-Lqq V or NBD-TTX to the sodium channel lead to a 35-fold enhancement in the fluorescence quantum yield, it was not necessary to remove unbound label as the contribution of the free signal to the cellular bound fluorescence emission is negligible. In the case of fluorescent derivatives of Lqq V, which bind to the channel in a voltage-dependent manner, the labeling was reduced greatly (to 7–10%) by depolarization of the cells with 135 mM external KCl or by dissipation of the membrane potential by the addition of 10 μg/ml gramicidin A (3). With CPM-Css II, TmRhd-Tityus γ, or NBD-TTX, specific binding was blocked by excess unlabeled toxin (2 μM).

For phospholipid labeling, either DiI or TmRhd-PE in ethanol (10 μg/ml with 0.1% ethanol) was added to the cells and incubated for 30 min at room temperature. FITC-s-concanavalin A (FITC-Con A) and TmRhD-wheat-germ agglutinin (TmRhd-WGA) were used at concentrations of 15 μg/ml and incubated with the cells for 30 min at room temperature. After this incubation the cells were washed five times with PBS for the remainder of the experiment.

Fluorescence Photobleaching Recovery (FPR)

Diffusion coefficients (D_L) and mobile fractions (f) of fluorescently labeled sodium channels were measured by the spot photobleaching technique using the apparatus described previously (7, 27). Measurements were carried out at 22°C. After equilibration of the fluorescent ligands and washing, the coverslip bearing the cells was inverted onto a serological plate that contained PBS. The monitoring Argon-ion laser beam (514, 488, or 457 nm, ~5 μW) was directed through a Zeiss Universal fluorescence microscope and focused with a 100× (1.3 NA) oil immersion objective to a Gaussian radius of 0.85 μm. In some experiments, 40× or 63× water immersion objectives were used and give beam radii of 1.8 or 1.3 μm, respectively. A brief pulse (5 mW, 10–200 ms) was used to bleach 60% of the fluorescence in the illuminated region. The time course of the fluorescence recovery was

followed using the attenuated monitoring beam. The lateral diffusion coefficient (D_L) and the mobile fraction (f), the fraction of the fluorescently labeled molecules that are mobile on the time scale of the experiment, were determined by curve-fitting procedures (7). Diffusion coefficients, D_L, in cm^2/s were determined from $w^2/4T_D$ in which w is the e^{-2} radius of the beam profile and T_D is the half-time for recovery (7). Incomplete fluorescence recovery is usually attributed to immobility of a fraction of the fluorophores on the time scale of the experiment (23). In our measurements fluorophores with $D_L \leqslant 2 \times 10^{-12}$ cm^2/s would appear immobile. Even if all the fluorophores are mobile, however, limiting the area of membrane that contains the observation region could also cause an incomplete recovery and therefore an apparent immobile fraction. In a closed and limited area, in contrast to the "infinite" area usually assumed in most treatments, a significant fraction of the total number of fluorophores could be bleached. Under this geometric constraint, complete recovery to the initial fluorescence would be impossible. However, the end result of measuring in a limited region would make the diffusion rate appear faster and the fractional recovery lower than in an infinite space. These considerations are discussed more fully in the Appendix and in relation to the mobility of sodium channels in the Discussion.

Nonspecific binding of the fluorescent toxin was measured by addition of fluorescent toxin together with excess unlabeled toxin (e.g., 200 nM Lqq V, 2 μM Css II, 2 μM Tityus γ, or 2 μM TTX) and measuring the fluorescent signal by photon counting for 4 s. No fewer than 20 cells in the culture were sampled in each region. These measurements were directly compared with cells to which only fluorescent toxin was added. In some experiments the nonspecific binding of TmRhd-Lqq V was measured after depolarization of the cells with 130 mM KCl replacing the choline chloride or 10 μg/ml gramicidin in a PBS medium. In addition, nonspecific fluorescence was evaluated by comparing the intensities from the neuronal cell membrane and from the substratum where sparse nonneuronal cells were observed.

Because there are slight variations in mobilities of fluorescent probes in FPR experiments, due primarily to cell-to-cell variations, a large number of measurements using at least 10 different culture preparations were used in statistical analyses to evaluate the differences between regions on the neuronal cell surface. Several FPR curves were obtained from each cell and preparation with each probe. From each curve two parameters, the characteristic diffusion time, T_D, and the degree of recovery of the bleached fluorescence, f, were obtained. Application of a modified student's t test gave a measure of the distinguishability of the mean value of T_D or f between the different cell regions (11). To avoid additional uncertainties due to beam size we measured each region on a single cell with a given probe such that no adjustments of the laser beam or the culture were required during the course of the experiments. Tables I and II and Fig. 3 show mean values for D_L and f, standard error of the mean, number of measurements for each region with each probe, and probability values for t test comparisons among regions. Each group of experiments was carried out on 10 separate occasions to control for variations in the conditions and quality of the cell cultures.

Results

Characteristics of Cell Cultures

Phase and differential interference contrast microscopy of mature cells (4–6 wk) reveal that the cultured neurons are dispersed on a background surface of nonneuronal cells. These neurons occurred often in isolation from other neurons in small groups or networks. (Figs. 1 and 2). Considerable cellular detail can be resolved including highly interconnected neurons with numerous long, highly branched cell processes or neurites. Areas of close contact between neighboring cells were common including varicosities and terminal swellings suggestive of synaptic contacts. In large neurons some of the terminal regions have discernable and identifiable boutons. Other laboratories have shown that these morphologically identifiable connections or appositions are correlated with a high degree of synaptic activity (28, 42). In addition, electrophysiological recordings from these regions have shown that the evoked excitatory postsynaptic potentials approximate a normal distribution with no evidence of preferred amplitudes as might occur with relatively low mean quantum content (28, 42). Of course at our level of morphology and microscopic resolution we cannot draw any definite conclusions as to the functional properties of each of these terminal structures, but for FPR measurements and for physiological exploration of cells regions, the visualization by phase or differential interference contrast microscopy provides a useful guide. Since we are not absolutely certain that each of these junctions serves as a functional presynaptic ending, we will use an operational definition and refer to this region only as the "neuritic terminal," where the neurite of one neuron meets the cell body of another neuron.

Binding of Fluorescent Neurotoxin Probes to Nerve Cells

Direct binding of ^{125}I-TmRhd-Lqq V or ^{125}I-TmRhd-Tityus γ to spinal cord neurons yielded K_ds of 6.5 and 4 nM, respectively with maximal binding capacities of 193 ± 26 and 214 ± 35 fmol/mg cell protein, respectively. This density corresponds to 116,000 sodium channels per cell on the average assuming a homogeneous distribution of channels (see below). The specificity of TmRhd-Lqq V binding to the cell surface was also determined by photon counting using the FPR system. Competition by 200 nM unlabeled Lqq V or by depolarization with KCl or gramicidin displaced 89 or 93% of the fluorescence, respectively, from the cells labeled with 10 nM TmRhd-Lqq V. Rough optical sectioning showed that >90% of the fluorescence originated from the cell membrane. This is to be expected since the neurotoxins are neither internalized nor inserted into the membrane due to their low lipid solubility and positive charges. The fluorescence remaining after displacement appears more homogeneously distributed and diffuse on the cell surface and represents nonspecifically bound toxin. This is also supported by the finding that prior fixation of the cells with 3% paraformaldehyde at 22°C for 1 h prevented the binding of 10 nM TmRhd-Lqq V but not the faint diffuse labeling.

Table I summarizes the specificity of the fluorescence labeling of spinal cord neurons at defined regions with a variety of fluorescent sodium channel neurotoxin probes. The level of nonspecific binding of TmRhd-Lqq and NBD-TTX in the presence of excess unlabeled toxin was 11 and 12%, respectively, compared with that seen in the absence of unlabeled toxin (Table I).

The dissociation of the fluorescent ligand during the experiment could also be measured by the decrease in the membrane-associated fluorescence intensity after dilution by washing. In the case of TmRhd-Lqq V or NBD-Lqq V the half-time for dissociation was 65 min at 22°C, which has been confirmed in experiments with ^{125}I fluorescently modified toxins (3, 17). Thus, the half-times for dissociation of these ligands are considerably longer than the time required for FPR measurements. Although TmRhd-Lqq V and NBD-Lqq V fluoresce in solution as well as when bound to the receptor, the spectral features of bound NBD-Lqq V are convenient because the signal from the specifically bound toxin is 35-fold higher than that from toxin in solution (3, 4). Therefore, the contribution to the signal from free ligand which has dissociated from the neuronal membrane is negligible.

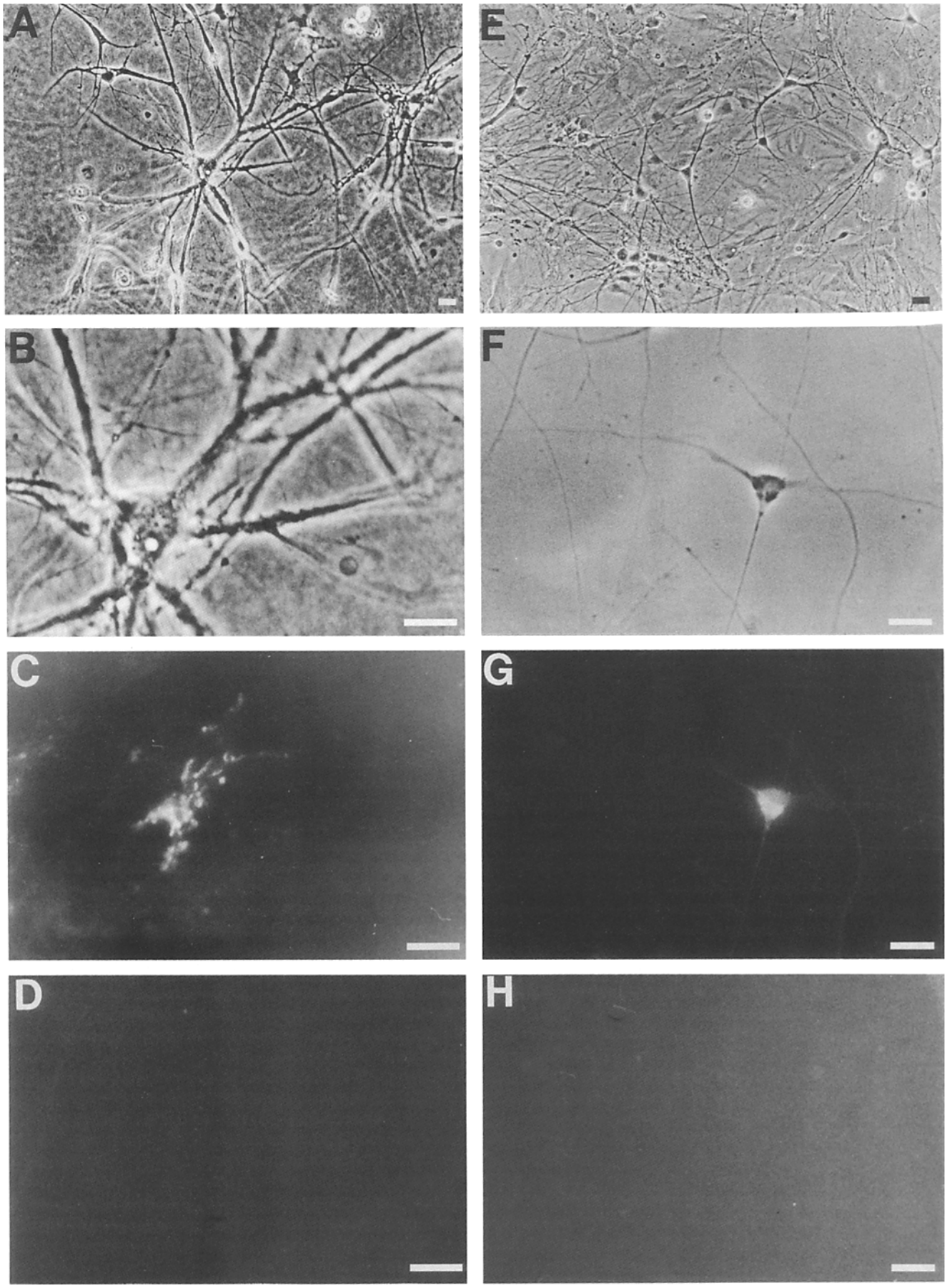
A
E
B
F
C
G
D
H

Distribution of Sodium Channels on Spinal Cord and Cortical Neurons

Fig. 1 shows the staining of sodium channels with fluorescent neurotoxins on spinal cord neurons (*A–D*) or cortical neurons (*E–H*) maintained in culture for 6 wk. After 2–6 wk in culture, these neurons could be labeled with fluorescent toxins whereas nonneuronal cells could not. Fig. 1 *C* shows the distribution of fluorescence on a large spinal cord neuron after labeling of voltage-dependent sodium channels with TmRhd-Lqq V with the focus on the plane of the neurite. The fluorescence staining over the cell body is faint and diffusely distributed compared with the more localized and punctate fluorescence of the labeled sodium channels observed at the axon hillock (Fig. 1 *C*). The staining is specific since it can be reduced by excess unlabeled toxin (Fig. 1 *D*). The same general staining pattern was observed with TmRhd-Tityus γ on cortical neurons (Fig. 1, *G* and *H*). In addition, cells underlying the neurons do not stain with the fluorescent toxins. To quantitatively map the topography and to test the generality of the distribution pattern in which higher fluorescence appears at the axon hillock compared with the cell body, cultures were scanned and scored quantitatively using the FPR apparatus (Table I). In 70% of the cells examined, the initial segment was four to five times more intensely labeled than the cell body, and seven to eight times more than the neuritic terminal. For the remaining 30% of the cells sampled the density of labeled sodium channels at the initial segment was 10–15 times greater than the cell body. This fluorescence-labeling pattern was blocked upon the addition of 200 nM unlabeled Lqq V, or by depolarization with 135 mM K^+ (Table I), or gramicidin A (Table I).

By comparison, when FITC-s-Con A, TmRhd-WGA receptors, or TmRhd-PE were examined, no pattern in the fluorescence labeling or levels of the fluorescence intensities (Table I) were observed indicating that for the bulk of lipids and glycoproteins, the distribution is homogeneous along the surface of the cell body, the axon hillock, and the neurite. In addition these results suggest that the increased fluorescence intensity from the sodium channel labeling was not due to localized foldings of the membrane which could enhance the fluorescence intensity by increasing the effective surface area. This is also supported by reports on the fine structure of these cells from other laboratories which have shown that there are no invaginations of the cell membrane around the axon hillock and that the cell surface is topographically uniform over all parts of the cell (42). To confirm that the punctate fluorescence and nonuniform labeling was due to sodium channels rather than the ligands per se, three different sodium channel probes, TmRhd-Lqq V, CPM-Css II (or TmRhd-Tityus γ), and NBD-TXX, each specific for a distinct receptor site on the sodium channel protein complex, were used (5). In all cases, the same nonuniform distribution of fluorescence was observed over the cell surface, consistent with the conclusion that this represents the distribution of the sodium channel protein.

Lateral Mobility of Voltage-dependent Sodium Channels on Nerve

The lateral mobility of sodium channels on two primary neuronal cultures was measured using a variety of sodium channel specific fluorescent probes. The FPR measurements were generally made at different regions on the same neuron: the cell body, the axon hillock, and the neuritic terminal.

Fig. 2 presents a series of typical FPR measurements on a single spinal cord neuron labeled with TmRhd-Lqq V. The recovery curves show significant differences in both the diffusion coefficients and fractional recoveries at various regions of the neuron. The results of many measurements are presented in Table II, which lists the diffusion coefficients and fractional recoveries of sodium channels measured with various specific labels at different regions of the same neuron. These results are summarized diagrammatically in Fig. 3. On the cell body most (~90%) of the labeled channels are mobile and diffuse relatively rapidly (D_L ~1–2 × 10^{-9} cm^2/s). In contrast, at the axon hillock and neuritic terminal the fractional recoveries are much lower (40 and 20%, respectively) and the mobile channels diffuse more slowly (D_L ~0.1–0.2 × 10^{-9} cm^2/s at both the axon hillock and neuritic terminal). Typically the failure of the fluorescence to recover to 100% of its prebleach level is attributed to the presence of labeled surface components which are immobile on the time scale of the measurements ($D_L \leq 2 \times 10^{-12}$ cm^2/s). Since the axon hillock and neuritic terminals are relatively small and present unique geometries, however, we have considered other explanations for the nonrecovering fractions and developed a theoretical treatment of the geometric constraints presented by the axon hillock (see Appendix). If the area of the membrane containing the observation region is small and closed (i.e., channels cannot diffuse into or out of the area), then a significant fraction of the total amount of fluorophore in the closed area could be depleted by photobleaching. Hence the fluorescence could not recover to its initial prebleach level even if all of the fluorophores in the area were mobile. As discussed below and in the Appendix the magnitude of the nonrecovering fraction of fluorescence in this situation depends on the relative sizes of the bleached area and the closed membrane area and on the extent of photobleaching. We tested this by comparing the fluorescence recovery after successive bleaches of the same hillock area. If the membrane area containing the observation region is closed, then successive bleaches will diminish

Figure 1. Fluorescence labeling of sodium channels by TmRhd-Lqq V on rat spinal cord (*A–D*) and by TmRhd-Tityus γ (*E–H*) on cortical neurons maintained in vitro for 6 wk. *A* and *B* are the phase micrographs of a spinal cord neuron and *E* and *F* are phase micrographs of the cortical neurons labeled. The nonspecific staining for Lqq V and Tityus γ are shown in *D* and *H*, respectively, where on a different cell the fluorescence has been reduced by depolarization of the cells by 135 mM K^+ (*D*) or 2 μM Tityus γ (*H*). The photographs were obtained with a Zeiss Photomicroscope III used in the FPR system where the laser served as the illumination source. The laser beam was dispersed by both a diffusion lens and an opaque rotating disk placed in the exciting light patch. The micrographs were recorded through a Zeiss 63× water immersion 1.2 NA objective on Tri-X film pushed to ASA 3200. Note the absence of staining of the underlying nonneuronal cells forming the substratum. Bar, 30 μm.

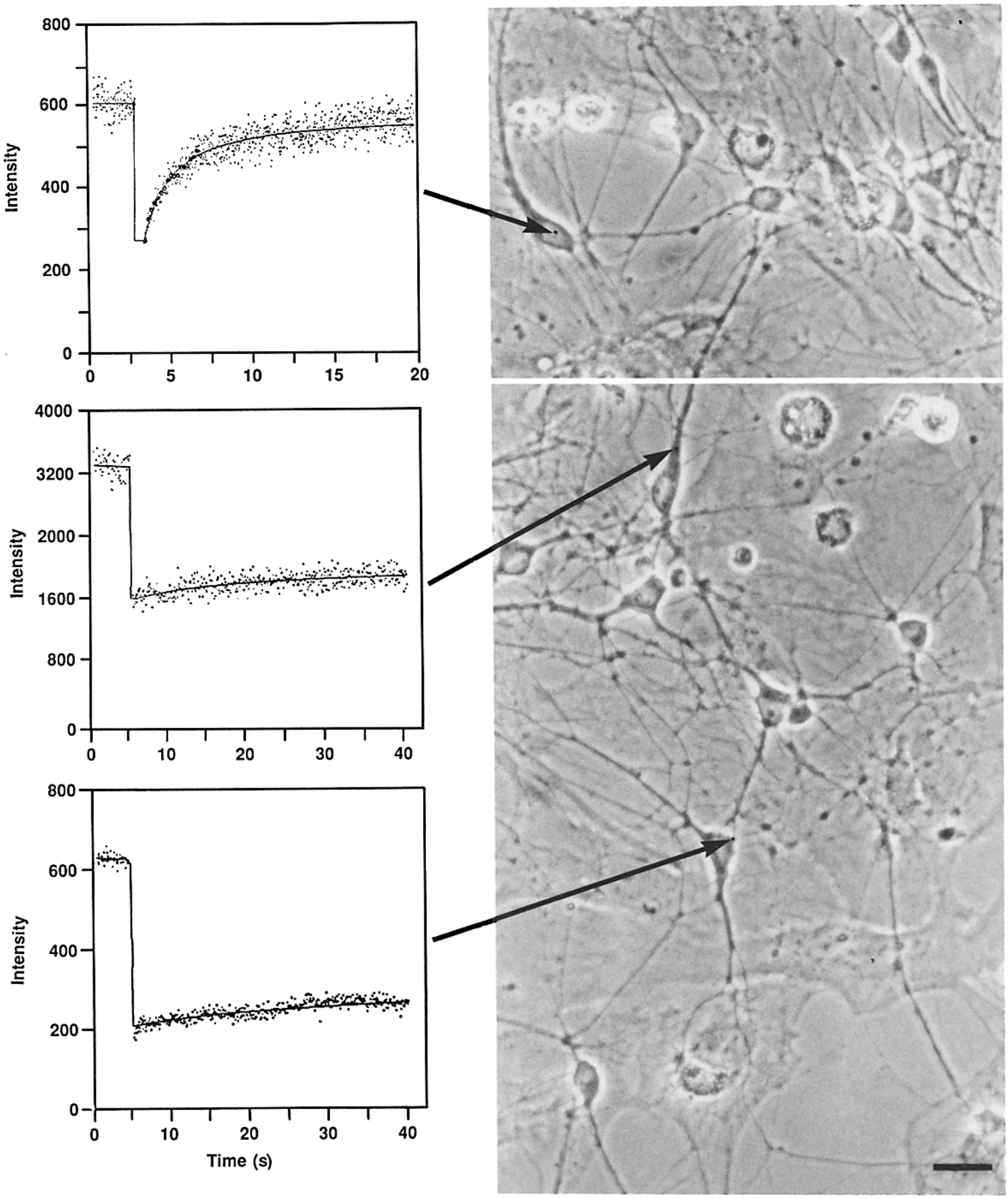
800
600
400
200
0
Intensity
0
5
10
15
20
4000
3200
2000
1600
800
0
Intensity
0
10
20
30
40
800
600
400
200
0
Intensity
0
10
20
30
40
Time (s)

Table I. Labeling of Spinal Cord Neurons with Fluorescent Sodium Channel Neurotoxins

Probe	Region	Concentration	Prebleach fluorescence intensity* Total	Nonspecific‡
		nM		
TmRhd-LqqV	Cell body	10	847 ± 45	91 ± 20
	Cell body	10	934 ± 80	64 ± 35§
	Hillock	10	3,556 ± 205	347 ± 45§
	Neuritic terminal	10	416 ± 104	70 ± 33
NBD-TTX	Cell body	10	525 ± 48	63 ± 25
	Hillock	10	2,370 ± 53	241 ± 83
	Neuritic terminal	10	330 ± 78	71 ± 24
TmRhd-LqqV Prior fixation	Cell body		93 ± 50	
	Hillock		191 ± 56	
	Neuritic terminal		81 ± 65	
No labeling	Cell body		45 ± 30	
	Hillock		37 ± 40	
	Neuritic terminal		51 ± 34	
FITC-s-Con A	Cell body	15 μg/ml	789 ± 158	
	Hillock	15 μg/ml	1,023 ± 397	
	Neuritic terminal	15 μg/ml	769 ± 163	
TmRhd-PE	Cell body	10 μg/ml	2,760 ± 120	
	Hillock	10 μg/ml	2,615 ± 164	
	Neuritic terminal	10 μg/ml	2,119 ± 260	

* Photon counts per 4 s. Fluorescence was measured from a 1.8- or 0.85-μm radius spot illuminated by the laser. 20–30 cells were scored in each entry and data are given as the mean and standard error of the mean. Within a given experiment with each probe the laser power and neutral density filters remained unchanged. The absolute levels, however, cannot be compared between FITC-s-Con A receptors and TmRhd-Lqq levels, since higher neutral density was used with FITC-s-Con A.

‡ Measured in the presence of 200 nM unlabeled LqqV or 2 μM TTX.

§ Depolarization with 10 μg/ml gramicidin.

the fluorescence toward zero. If mobile fluorophores can diffuse onto the hillock from the cell body, then the final fluorescence after several bleaches should be no less than that contributed by the mobile fluorophores. We can consider two idealized illustrations of how fluorophores might be restricted: (*a*) all the fluorophores are mobile, but the membrane area is small and closed or (*b*) the membrane area is infinite (i.e., mobile channels can diffuse unhindered from the cell body to the axon hillock), but, as suggested by our measurements, 60% of the channels are immobile. In the former case, since 40% of the channels are unbleached (we usually bleached 60% of the channels), and the recoverable fraction of channels was 0.4, then we can calculate the amount of prebleach fluorescence that should remain after each photobleach and recovery; 40% (unbleached) + 0.4 (recoverable fraction) + (60%) = 64% of the prebleach fluorescence would be present after each photobleach and recovery, or after three successive photobleaches would be about $(0.64)^3$ or 26% of the initial prebleach level. In the second case, since 40% of the labeled molecules are mobile, and assuming diffusion into the hillock area from the cell body, the final fluorescence would be at least 40% of the initial level. (The residual unbleached immobile fluorophores add another ~4% so that the final fluorescence after recovery from the third photobleach would be ~44% of the initial value.) Experimentally we observed that the fluorescence was reduced to ~10% of its initial prebleach level by three successive photobleaches. This suggests that the area of the axon hillock is closed to diffusion of sodium channels from the cell body although there could, in addition, be some immobile channels in the hillock region. If the area of the axon hillock is closed to diffusion of channels across its boundaries, this would also have an effect on the apparent diffusion rates of the mobile channels. As discussed in the Appendix, if the closed area has a relatively compact shape (i.e., approximated by a square or circle rather than by a long thin rectangle), and supposing that the diffusing channels are simply reflected by the boundary, then the apparent diffusion rate will be faster than for an unbounded region. Hence, the diffusion coefficient calculated for a supposed unbounded re-

Figure 2. Representative FPR curves of TmRhd-Lqq V on spinal cord neurons. Cells were labeled with 10 nM ThRhd-Lqq V as described above and FPR measurements were performed at 22°C. The points represent photons counted per 40-ms dwell time. Solid lines are the computer-generated nonlinear regression best fit fluorescence recovery curves obtained for a lateral diffusion process with a single diffusion coefficient, D_L. Photobleaching on the cell body (*top*), axon hillock (*center*), and at the neuritic terminal or contact region between two nerve cells (*bottom*) using a 0.85-μm beam radius (100×) objective. The right hand panels show the location of the photobleaching spot on a phase-contrast image of a nerve cell preparation. The diffusion coefficients are 1.8×10^{-9} cm²/s at the cell body, 1.1×10^{-10} cm²/s at the axon hillock, and 1.6×10^{-10} cm²/s at the terminal with fractional recoveries of 0.9, 0.31, and 0.22, respectively. Bar, 50 μm.

Table II. Regionalization and Mobility of Sodium Channels

Probe	Cell type	Region	$\langle D \rangle + D$ $\times 10^{-9}$ cm²/s	$\langle f \rangle \pm f$	n
TmRhd-Lqq V	Cort neuron	Cell body	1.84 ± 0.75	0.83 ± 0.1	80
NBD-Lqq V	Cort neuron	Cell body	1.35 ± 0.82	0.77 ± 0.07	17
TmRhd-Lqq V	Spinal cord	Cell body	1.05 ± 0.32	0.89 ± 0.15	45
TmRhd-Lqq V +WGA	Spinal cord	Cell body	0.96 ± 0.21	0.87 ± 0.12	8
NBD-TTX	Spinal cord	Cell body	1.98 ± 0.74	0.86 ± 0.17	8
CPM-Css II	Spinal cord	Cell body	2.21 ± 0.53	0.89 ± 0.15	5
TmRhd-Con A	Cort neuron	Cell body	0.02 ± 0.008	0.19 ± 0.13	11
TmRhd-WGA	Spinal cord	Cell body	0.79 ± 0.12	0.19 ± 0.11	12
FITC-s-Con A	Cort neuron	Cell body	0.41 ± 0.07	0.39 ± 0.11	4
FITC-s-Con A	Spinal cord	Cell body	0.62 ± 0.13	0.48 ± 0.10	6
TmRhd-PE	Spinal cord	Cell body	7.2 ± 0.38	0.95 ± 0.07	21
DiI	Spinal cord	Cell body	6.6 ± 0.7	0.83 ± 0.06	10
TmRhd-Lqq V	Cort neuron	Hillock	0.19 ± 0.06	0.42 ± 0.17	56
TmRhd-Lqq V	Spinal cord	Hillock	0.15 ± 0.08	0.38 ± 0.15	75
TmRhd-Lqq V +WGA	Spinal cord	Hillock	0.12 ± 0.06	0.31 ± 0.11	8
CPM-Css	Spinal cord	Hillock	0.11 ± 0.09	0.41 ± 0.13	8
TmRhd-Con A	Cort neuron	Hillock	0.04 ± 0.009	0.13 ± 0.11	11
TmRhd-WGA	Spinal cord	Hillock	0.19 ± 0.009	0.28 ± 0.08	7
FITC-s-Con A	Spinal cord	Hillock	0.39 ± 0.04	0.16 ± 0.04	8
TmRhd-PE	Spinal cord	Hillock	5.8 ± 1.2	0.83 ± 0.11	11
DiI	Spinal cord	Hillock	7.8 ± 0.8	0.87 ± 0.09	10
TmRhd-Lqq V	Cort neuron	Neuritic terminal	0.21 ± 0.11	0.20 ± 0.09	46
TmRhd-s-Con A	Cort neuron	Neuritic terminal	0.92 ± 0.31	0.76 ± 0.15	6
TmRhd-PE	Spinal cord	Neuritic terminal	5.55 ± 1.2	0.89 ± 0.17	11
DiI	Spinal cord	Neuritic terminal	6.2 ± 0.6	0.76 ± 0.05	10

Table III. t Tests for Significant Differences in Interregional $\langle D \rangle$ and $\langle f \rangle$

Regions	Probe	Parameter	t for difference	Probability that difference is significant	Parameter	t for difference	Probability that difference is significant
				%			%
Body/hillock	TmRhd-Lqq V	*D*	5.58	>99.7	*f*	7.02	>99.9
Body/synapse	TmRhd-Lqq V	*D*	5.04	>99.7	*f*	10.22	>99.9
Hillock/synapse	TmRhd-Lqq V	*D*	1.58	>70	*f*	3.79	>90
Body/hillock	FITC-s-Con A	*D*	1.86	>90	*f*	1.27	>70
Body/synapse	FITC-s-Con A	*D*	0.33	>65	*f*	1.71	>80
Hillock/synapse	FITC-s-Con A	*D*	2.41	>95	*f*	0	0
Body/hillock	TmRhd-PE	*D*	0.80	>50	*f*	0.99	>50
Body/synapse	TmRhd-PE	*D*	1.44	>75	*f*	1.07	>60
Hillock/synapse	TmRhd-PE	*D*	0.37	>60	*f*	0.27	>40

gion will be a lower bound to the actual rate of diffusion in an appropriately shaped closed region. Thus consideration of the geometry of the axon hillock region as a relatively compact area shows that the diffusion coefficient measured would appear faster than it would in an infinite space and thus the actual lateral mobility of sodium channels in the hillock would be slower than 0.1–0.2 $\times 10^{-9}$ cm²/s. Therefore the geometry of the hillock cannot account for the measured retardation in the diffusion rate of sodium channels in the axon hillock reported here. Our conclusion that sodium channel diffusion in the hillock is slower than on the cell body is not changed by supposing that the hillock-soma boundary is closed to channel diffusion.

Both Table III and Fig. 3 show that the probability that the observed differences between the cell body and axon hillock and cell body and neuritic terminal are significant is >99.7%. The diffusion coefficients for channels measured at each region are in the range reported for other intrinsic membrane proteins (13), although sodium channels on the cell body are at the upper end of the range for cell surface proteins measured by FPR.

In some experiments, we used rabbit anti-channel TmRhd-Fab'. Although the diffusion coefficients were approximately the same, the nonspecific labeling with TmRhd-Lqq V (11 ± 4%) is lower than that with TmRhd-Fab' (20 ± 8%) since preparation of the Fab' fragment results in some loss of antibody affinity. Since the fluorescent neurotoxin has a higher affinity than the Fab', and the nonspecific binding can be de-

termined directly from the same culture by depolarization, the neurotoxin derivatives appear to be superior FPR probes. The use of different sodium channel probes (e.g., Lqq V, TTX, and Css II [or Tityus γ]) that bind to the sodium channel protein at independent and topographically distinct sites (4–6, 17), and the demonstration that the diffusion coefficients are independent of the probe used, tend to eliminate any biasing or artifactual contributions from the probes themselves. Controls in which fluorescently labeled cells were fixed with 3% paraformaldehyde essentially immobilized the labeled channels. This immobilization verifies that the rapid fluorescence recovery observed with unfixed cells corresponds to the sodium channel mobility and not some form of ligand surface "hopping." Furthermore, the rapid recovery rate, particularly that measured on the cell body, is considerably faster than the rate constant for ligand dissociation, and therefore does not reflect the kinetics of ligand association/dissociation from the cell surface.

The restriction of the diffusion of sodium channels from cell body to axon hillock suggests that the lipid bilayer component of the membrane might have different fluidity characteristics in different regions of the neuron due, for example, to partitioning of phospholipids into domains (29). Measurements of the diffusion of the lipid probe TmRhd-PE or DiI, however, revealed no regional differences on spinal cord neurons (Tables II and III). The fluorescent phospholipid derivatives diffused freely in all membrane regions examined with a high diffusion coefficient of 5–7 × 10^{-9} cm^2/s, characteristic of these lipid probes (13, 45, 46). Hence inhomogeneities in the membrane lipid viscosity cannot account for the differences in channel diffusion rates observed in different regions of the neurons, and any barriers that restrict sodium channel diffusion from the cell body to the axon hillock do not influence diffusion of lipids.

To find out whether the interregional differences in mobilities for sodium channels was also characteristic of other proteins, we measured and compared the mobilities of TmRhd-WGA and FITC-s-Con A receptors on the membranes of cortical and spinal cord neurons. Tables II and III show that there are no significant differences in the diffusion coefficients of TmRhd-WGA or FITC-s-Con A at the cell body, axon hillock, or synapse, although the corresponding mobile fractions are slightly less at the initial segment. The lateral diffusion coefficients measured for the lectin receptors are ~10% of that of TmRhd-PE and are in the range which is characteristic for many membrane proteins (46).

To investigate whether anchorage modulation (27) had any role in controlling the lateral mobility of sodium channels we examined the effects of cross-linking by WGA. Administration of this ligand had no significant effect on either the diffusion coefficient or fractional recoveries. A slight decrease in the total mobile fraction at the axon hillock but none at the cell body was observed, however, when WGA, which binds tightly to the sodium channel protein, was applied (Table II). This suggests a WGA-induced aggregation or cross-linking of the previously segregated sodium channels in this region.

We also examined the effects of colchicine (10^{-5} M) and cytochalasin B (100 μg/ml), agents known to affect cytoplasmic microtubules and microfilaments. There were no differences in either the measured diffusion coefficient or fractional recovery in any region indicating that these elements

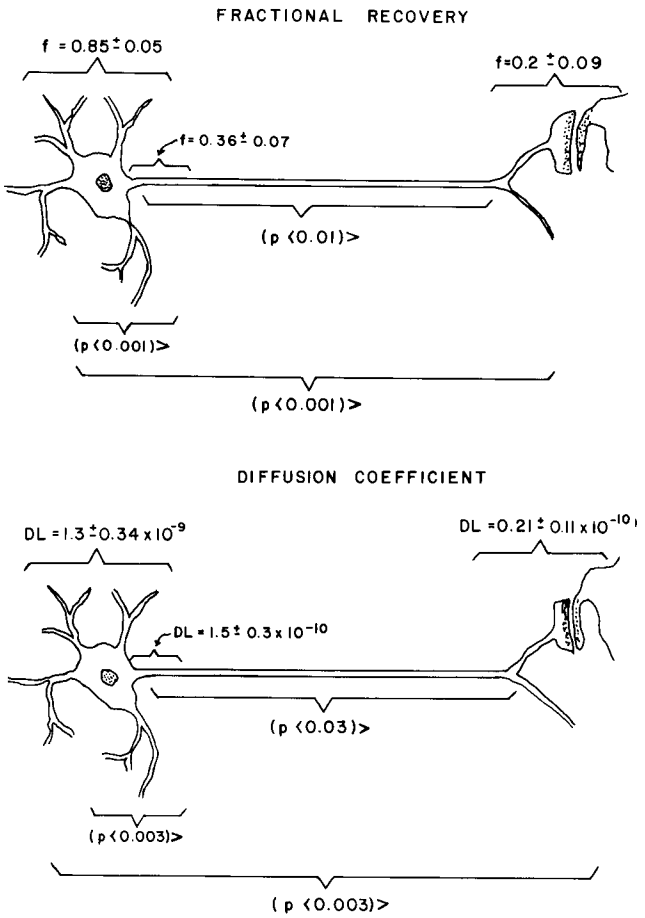

Figure 3. Significance of differences of observed values of diffusion coefficients (D_L) and fractional recovery (f) between various regions of the neuron. The arrows delineate the regions compared, and the P values are given in parentheses. Direction of difference is indicated by > or < after P values. The mean values of D_L and f are given in the various regions of the neuron, as measured by FPR experiments with TmRhd-Lqq V as the probe. See Table III.

are probably not directly involved in controlling sodium channel lateral mobility.

Table II shows that some uncertainties are associated with the experimental results. In some instances the relatively large standard error of the mean listed may be due to variation from different cell preparations, from cell to cell, or from one region to another on the same cell in addition to random measuring errors. Nevertheless, t tests show that significant differences exist between these regions. The largest difference that we observed, for example, were fractional recoveries of 89 and 57% of TmRhd-Lqq V on the cell body measured in single culture plates on two separate occasions. The diffusion coefficients, however, were in good agreement, 2.20 × 10^{-9} cm^2/s and 2.5 × 10^{-9} cm^2/s.

Discussion

A neuron is a highly asymmetric cell with a heterogeneous distribution of proteins along its plasma membrane. For some time it has been known that the axon exhibits a high degree of regional specialization in its electrical properties linked to the diverse physiology of the neuron (15). Hence,

to understand neuronal development it is important to learn how the regional differentiation of its surface arises and is maintained. Up to now this problem has been studied principally with methods that provide a static picture of the distribution of membrane components. Ultrastructural examination of the axonal membrane has revealed a heterogenous distribution of intracellular organelles and plasma membrane components (21, 44, 50, 57). Cytochemical, morphological, and biochemical studies have suggested that particles identified with sodium channels (IMPs) are clustered at discrete regions of the axolemma (19, 20, 44, 57, 59–60). The nature of the constraints which confine membrane components to specific locations is unknown. Originally it was thought that in myelinated axons the junction between an axon and its glia or Schwann cell was sufficient to confine sodium channels to the nodal region (44). Recent studies, however, show that heminodes and amyelinated sections of dystrophic mouse nerve contain particle patches having size density distributions similar to that of normal membranes. This suggests that sodium channels and other particles are confined to the nodal region by other constraints (19).

Measurements of the rates of lateral diffusion of sodium channels in various regions of the neuron surface should help to characterize the constraints that confine sodium channels to the regions. One approach has been to measure distribution of intramembrane particles (which are correlated with sodium channels) by electron microscopy and to calculate diffusion coefficients assuming perikaryal insertion and diffusion along the growing axolemma (49, 50, 52). There is, however, some uncertainty whether the IMPs represent voltage-dependent sodium channels.

Using fluorescence photobleaching recovery and channel-specific neurotoxins we have taken a direct approach to measuring sodium channel mobility and distribution on living cells. The heterogeneity of sodium channel distribution is seen in the micrographs and in the quantitative data in Table I. Compared with the cell body there is a higher density of channels in the axon hillock and a lower density in the neuritic terminal. The diffusion coefficient of sodium channels on the cell body is at the high end of the range observed for membrane proteins (13). Taking into account the measurements on TmRhd-PE, the channels diffuse at a rate close to that expected for a membrane protein limited only by the viscosity of the lipid bilayer (45). Similar diffusion coefficients have been measured for the acetylcholine receptor in embryonic muscle using a nonfluorescence method (39), rhodopsin in amphibian rod outer segment disks (40), for some surface antigens such as H-2Ld (18) and the antigen restricted to the posterior tail region in guinea pig sperm (PT-1) (37), and for plasma membrane proteins in which the underlying cytoskeleton may be modified or is separated from the membrane (54).

In contrast to the cell body the axon hillock region of the neuron displays a patchy pattern of fluorescently labeled sodium channels which are constrained to the axon hillock and diffuse significantly more slowly than sodium channels on the cell body (Table II). Hence motion of sodium channels must be retarded by forces in addition to the viscosity of membrane bilayer. The forces could arise from several kinds of interactions within the plasma membrane or between the membrane and the cytoskeleton: (*a*) The channels might interact directly with the specialized cytoskeleton present in this region of the cell (21). An example of this kind of interaction occurs in erythrocytes in which the diffusion of the band 3 protein is retarded due to interactions with spectrin via the linking protein, ankyrin (38). (*b*) The channel might interact with other membrane proteins which in turn interact with the cytoskeleton. This seems to occur with stearoyl dextrans inserted into cell membranes (61) and with histocompatibility antigens from which the cytoplasmic domain has been deleted (16). (*c*) The channel might interact sterically with other proteins, which are present at high concentrations in the plasma membrane. This kind of interaction typically seems to have only a weak effect on membrane protein diffusion but may have been observed for IMPs in regenerating axon membranes (49). (*d*) The channel might be preferentially concentrated into membrane lipid domains (29) with very high viscosity.

The different rates of diffusion of sodium channels and FITC-s-Con A receptors on the cell body indicate that a substantial fraction of the proteins in this membrane region experience stronger retarding interactions than do sodium channels. Hence the forces that retard protein diffusion on this part of the plasma membrane must have some measure of molecular specificity.

It seems likely that the forces that retard diffusion also contribute to the regional localization of the channels. It also appears, however, that an impermeable barrier between the axon hillock and the cell body prevents transfer of the channels between regions (without limiting their diffusion within the regions). Thus it seems that the soma–hillock annulus imposes a barrier to the diffusion of specific proteins such as sodium channels while allowing other proteins and lipids to diffuse freely between these regions. The existence of this kind of barrier is suggested by the net depletion of fluorescence from labeled channels in the axon hillock after several bleaches. Furthermore, electron micrographs reveal that a dense cytoskeletal matrix, a submembranous electron dense region, and a concentration of small IMPs on the P-face of the membrane occur at the soma–hillock junction (31, 41, 44, 57, 59, 60). The very dense staining in thin sections of mammalian nodes termed the subaxolemmal undercoating (21) might constrain channel mobility. Electron microscopic observation demonstrates that a three-dimensional network of interwoven filaments, is firmly attached to the axolemma. Another possible example of a selective barrier to diffusion comes from studies of the PT-1 antigen on sperm cells which is confined to but diffuses freely in the posterior tail region (37).

Confinement of sodium channels to localized regions could also result from interactions between the axon cell surface and the extracellular matrix including the basal lamina provided by glial cells. A similar situation may occur in innervated skeletal muscle where sarcolemmal channels appear immobile and congregated in patches (2, 53). Moreover it has been shown that formation of basal lamina and the appearance of laminin is important in Schwann cell proliferation and for maturation of the axolemmal membrane (12, 32).

Restriction of sodium channel mobility at neuritic terminals might occur by mechanisms similar to those proposed for the axon hillock region although cell–cell contacts and interactions with extracellular components specific to these regions may also contribute (14, 58). The extensive glycosylation of the channel protein, which is required to maintain

functional sodium channels in neuroblastoma cells (56), may also be involved in confining channels to specific cellular regions. Recent studies have shown that both fodrin (34) and ankyrin isoforms copurify with the sodium channel protein from rat brain synaptic endings despite several affinity chromatographic steps (e.g., lectin chromatography and sucrose gradients) and binds in a 1:1 stoichiometry with the purified and reconstituted sodium channel protein (51). In addition, the [^{3}H]saxitoxin-binding activity associated with the sodium channel can be immunoprecipitated with antiankyrin antibodies in the presence of added ankyrin. Hence there may be a linkage of sodium channels to the neuronal cytoskeleton either directly or via an intermediate such as brain ankyrin. In this connection, differences in the cytoplasmic distribution of $\alpha\gamma$ (fodrin) and $\alpha\beta$ neuronal spectrins (33) may be pertinent and may contribute to the segregation of ankyrin and sodium channel isoforms on the axonal surface.

The segregation and lateral mobility of sodium channels shows some specificity since measurements of other ion channels in these nerve cell preparations show quite different regionalizations and lateral mobilities. For example, measurement of the distribution and lateral mobility of benzodiazepine/γ-aminobutyric acid receptor on spinal cord neurons (55) show that these receptors are largely restricted to the cell body and are immobilized there while sodium channels are freely mobile in this region.

Measurements of sodium channel distribution and mobility in muscle have also been performed using UV photobleaching through patch-clamp pipettes and electrophysiological techniques (10, 53). Recently, Beam et al. (10), using the loose patch-clamp technique, have found a high sodium current density localized to the endplate which falls off rapidly with increasing distance from this region. Using these neurotoxin probes, we have shown that innervation induces sarcolemmal sodium channels to redistribute at neuronal contact sites and to become immobilized at the synapse (2).

In conclusion, we have observed that sodium channels are present at substantially higher surface density at the axon hillock relative to the cell body and that this difference correlates with substantial reduction of the lateral mobility of the channels. We think it likely that the forces that are responsible for these differences in mobility also participate in confining the channels to specific regions. Barriers that restrict the diffusion of channels but not of lipid between cell body and axon hillock also seem to be involved. Whatever the mechanisms by which sodium channels are regionally restricted, a major concern is how this regionalization and immobilization is regulated in development. By examining neuronal systems that are undergoing rapid neurite extension, neurons that form functional connections with muscle, or neurons undergoing myelination, it should be possible to gain further insights into the mechanisms and signals that segregate and maintain sodium channels at discrete regions on the neuronal cell surface.

Appendix I

Measurement of Diffusion in Closed Region by FPR

Measurements in the foregoing paper suggest that Na^+ channels are prevented from diffusing from the cell body onto the hillock. Confinement of the channels on the hillock to a small region could affect the interpretation of the FPR measurements. Therefore, in this Appendix we consider the effects on the apparent diffusion coefficient and fractional recovery of limiting the area available to the diffusant.

Since we are uncertain of the size and shape of the region to which the channel molecules on the hillock are confined, we shall, for simplicity, consider a rectangular region bounded by $\pm L_x$ and $\pm L_y$ on the x- and y-axes. As is typical for spot photobleaching experiments, the excitation intensity profile is a Gaussian centered at the origin of the coordinates and with an exp(−2) radius of w. Our objective is to calculate $\delta F(t)$, the difference between the initial prebleach fluorescence and the fluorescence at time t, having specified the parameter, κ, which defines the extent of bleaching (8). Using standard Fourier transform methods it can be shown that

$$\delta F(t) = \frac{-16Q\bar{c}I_0}{L_x L_y} \sum_{v=1} \frac{(-\kappa)^v}{v_!} \left\{ \sum_{\substack{n_x=0 \\ n_y=0}} A(n_x, n_y) \right.$$

$$\exp\left\{ -\left[\left(\frac{n_x}{L_x}\right)^2 + \left(\frac{n_y}{L_y}\right)^2\right]\pi^2 Dt\right]\right\}$$

$$\times \int_0^{L_x} \exp\left[\frac{-2v\xi^2}{w^2}\right] \cos\left(\frac{n_x\pi\eta}{L_x}\right) d\zeta \int_0^{L_x}$$

$$\exp\left[\frac{-2x^2}{w^2}\right] \cos\frac{n_x\pi x}{L_x}\, dx \qquad \textbf{(A1)}$$

$$\times \int_0^{L_y} \exp\left[\frac{-2v\eta^2}{w^2}\right] \cos\left(\frac{n_y\pi\eta}{L_y}\right) d\eta \int_0^{L_y}$$

$$\left.\exp\left[\frac{-2y^2}{w^2}\right] \cos\frac{n_y\pi y}{L_y}\, dy \right\}$$

where $A(n_x,n_y) = 1$ for $n_x, n_y \neq 0$; $A(n_x,n_y) = 1/2$ for $n_x = 0$, $n_y \neq 0$ or $n_x \neq 0$, $n_y = 0$; and $A(n_x,n_y) = 1/4$ for $n_x, n_y = 0$. In this equation Q is a factor which accounts for the optical properties of the fluorophore and geometrical and loss factors determined by the experimental apparatus; $\bar{c}$ is the equilibrium concentration of the fluorophore before photobleaching; I_0 is the intensity of the monitoring excitation intensity at the origin of coordinates; and D is the diffusion coefficient of the fluorophores. Fig. A1 displays the effect of

This appendix prepared by Hong Qian and Elliot L. Elson, Department of Biological Chemistry, Washington University School of Medicine, St. Louis, Missouri 63110.

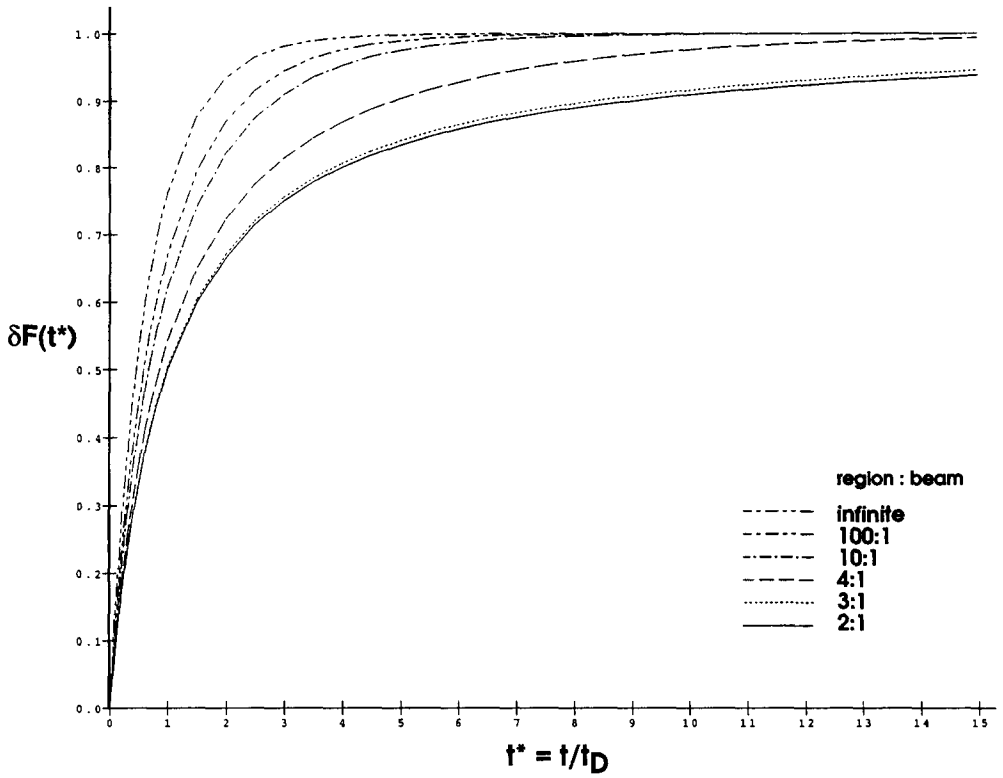

Figure A1. Dependence of FPR recovery on area available for probe diffusion. Recovery curves were calculated for square areas using Eq. A1. The amplitudes of the curves are normalized so that each curve reaches unity at $t = \infty$. The values of $\delta F(t^*)$ were plotted relative to a normalized time, $t^* = t/t_D$ where $t_D = w^2/4D$. The areas of the diffusion space, L_xL_y, relative to (w^2) are given on the figure.

the area of the square sample area on the apparent recovery rate. For these calculations $w = 1$ μm, and so the beam area is ~3.14 μm². It is clear from this figure that the apparent diffusion rate increases relative to that for an infinite area as the same area diminishes. This increase in apparent rate can be understood as a consequence of the elimination from the recovery process in the small area of the slow contributions due to diffusion from remote points. Hence, for relatively compact regions such as squares, limitation of the available area makes the diffusion appear faster than it would in an

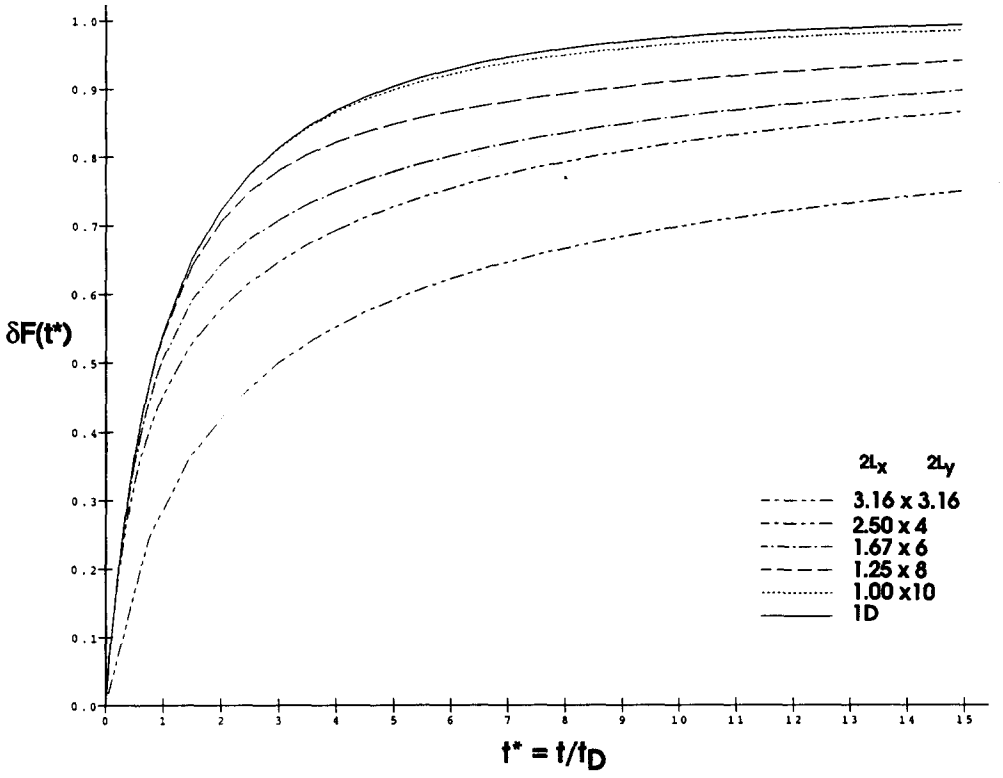

Figure A2. Dependence of FPR recovery on shape of area available for probe diffusion. Recovery curves were calculated for rectangular regions with different ratios of L_x to L_y, keeping the area of the regions constant at 10 square units where the beam radius $2w = 2$ U. As in Fig. A1 the recovery is plotted versus normalized time and amplitudes are adjusted to reach unity at $t = \infty$. The ratios of L_x to L_y are shown on the figure.

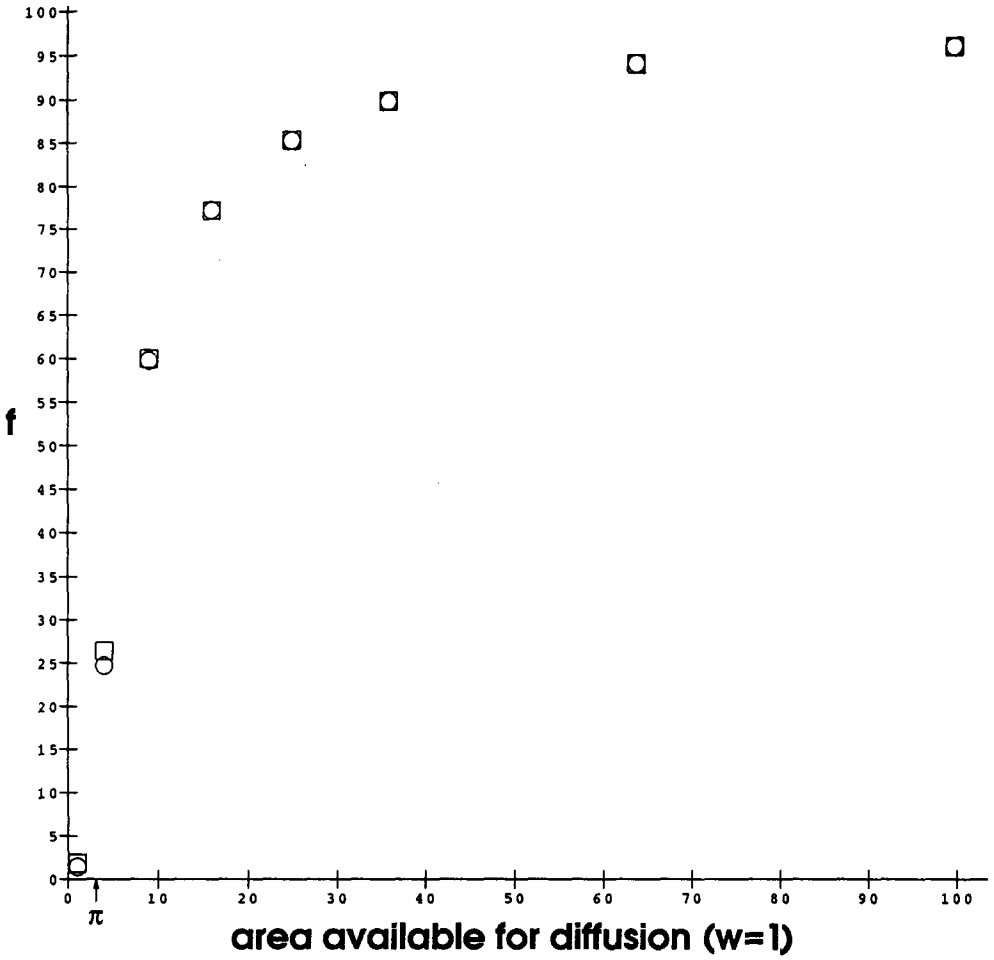

Figure A3. Dependence of fractional recovery on the area available for probe diffusion. Fractional recoveries were calculated as described in the Appendix. The bleached area is π on this scale; the beam radius $w = 1$. (□) Square region; (○) circular region.

infinite space and so cannot account for the measured retardation in the diffusion rate of channels in the hillock which are reported in this paper. This conclusion must be qualified, however, by the recognition that the shape of the confined area can also influence the apparent diffusion rate. This is shown in Fig. A2 which presents recovery curves calculated for rectangular regions with the same area but different ratios of L_x to L_y. In elongated regions the recovery process includes contributions from remote points, and so the apparent diffusion rate is retarded relative to compact regions with the same area. In principle, then, the measured slow fluorescence recovery on the hillock might be attributed to diffusion of channels from relatively distant points on the axon onto the hillock. We cannot assess quantitatively the magnitude of this effect, but we expect it to be negligibly small due to the low level of channels on the axon. These conditions do not affect our conclusion that diffusion from the soma to the hillock is blocked.

Confinement of fluorophores to a closed area of size comparable to the bleached region enables the photobleaching pulse to eliminate a significant fraction of the fluorophores in the region and thereby to diminish the fractional recovery even if all the fluorophores are rapidly mobile. Evidently this reduction in fractional recovery increases as the ratio of bleached area to total sample area and the extent of photobleaching (measured by κ) increase. The fractional recovery, f, can be represented as follows:

$$f = [F(\infty) - F(0)]/[F(<0) - F(0)]$$

where $F(<0)$, $F(0)$, and $F(\infty)$ are the measured fluorescence before, just after, and at long times after the photobleaching pulse, respectively.

For a $2L_x$ by $2L_y$ rectangular region,

$$F(<0) = J\, erf(L_x\sqrt{2}/w)\, erf(L_y\sqrt{2}/w)$$
$$F(0) = -J/\kappa \sum_{n=1} (-\kappa)^n/n!\, erf[L_x\sqrt{(2n)}/w]\, erf[L_y\sqrt{(2n)}/w]$$
$$F(\infty) = F(<0)\{1 + (\pi w^2)/(2L_xL_y) \sum_{n=1} (-\kappa)^n/(nn!)\, erf[L_x\sqrt{(2n)}/w]\, erf[L_x\sqrt{(2n)}/w]\}.$$

Where $erf(z)$ represents the error function of z; $J = Q\check{c}I_0\pi w^2/2$; and κ has been defined above.

For a circular region of radius R,

$$F(<0) = J[1 - \exp(-2R^2/w^2)]$$
$$F(0) = -(J/\kappa)\{\exp(-\kappa) - \exp[-\kappa\exp(-2R^2/w^2)]\}$$
$$F(\infty) = F(<0)\{1 = (w^2/2R^2) \sum_{n=1} [(-\kappa)^n/(nn!)\ 1 - \exp(-2nR^2/w^2))]\}.$$

Fig. A3 plots the fractional fluorescence recovery versus area of the space available for fluorophore diffusion assuming that all fluorophores are mobile. The photobleaching parameter κ is chosen to be 2.0 to yield fractional bleaches comparable to those obtained experimentally on labeled channels. Evidently the fractional recovery depends significantly on the shape of the available area only for very small areas. If we supposed that all labeled channels in the hillock were fully mobile, then, based on Fig. A2, the observed value $f = 0.4$ suggests that the area available to channels on the hillock is only slightly greater than the bleached area, πw^2.

This work was supported by the National Institutes of Health (NIH) grant NS 24606 and a Research Career Development Award (NS 01218) to K. J. Angelides; NIH grant GM 30299 to E. Elson; and a grant from the Muscular Dystrophy Association to K. J. Angelides. L. W. Elmer is a NIH Postdoctoral Fellow (NS 08224).

Received for publication 11 July 1987, and in revised form 10 January 1988.

References

1. Angelides, K. J. 1981. Fluorescent and photoactivatable fluorescent derivatives of tetrodotoxin to probe the sodium channel of excitable membranes. *Biochemistry.* 20:4107–4118.
2. Angelides, K. J. 1986. Fluorescently labelled Na^+ channels are localized and immobilized to synapses of innervated muscle fibres. *Nature (Lond.).* 321:63–66.
3. Angelides, K. J., and T. J. Nutter. 1983. Preparation and characterization of fluorescent scopion toxins from *Leiurus quinquestriatus* as probes of the sodium channel of excitable cells. *J. Biol. Chem.* 258:11948–11957.
4. Angelides, K. J., and T. J. Nutter. 1983. Mapping the molecular structure of the voltage-dependent sodium channel: distances between tetrodotoxin and *Leiurus quinquestriatus* scorpion toxin receptors. *J. Biol. Chem.* 258:11958–11968.
5. Angelides, K. J., and G. B. Brown. 1984. Fluorescence resonance energy transfer on the voltage-dependent sodium channel: spatial relationship and site coupling between the batrachotoxin and *Leiurus quinquestriatus* α-scorpion toxin receptors. *J. Biol. Chem.* 259:6117–6126.
6. Angelides, K. J., and T. J. Nutter. 1983. Molecular and cellular mapping of the voltage-dependent sodium channel. *Biophys. J.* 45:31–34.
7. Axelrod, D. 1983. Lateral motion of membrane proteins and biological function. *J. Membrane Biol.* 75:1–10.
8. Axelrod, D., D. E. Koppel, J. Schlessinger, E. L. Elson, and W. W. Webb. 1976. Mobility measurement of analysis of fluorescence photobleaching recovery kinetics. *Biophys. J.* 16:1055–1069.
9. Barchi, R. L. 1983. Protein components of the purified sodium channel from rat skeletal muscle sarcolemma. *J. Neurochem.* 40:1377–1385.
10. Beam, K. J., J. H. Caldwell, and D. J. Campbell. 1985. Na^+ channels in skeletal muscle are concentrated near the neuromuscular junction. *Nature (Lond.).* 313:588–560.
11. Bevington, P. R. 1969. Data Reduction and Error Analysis for the Physical Sciences. McGraw-Hill, Inc., New York. 33611 pp.
12. Bunge, M. B., A. K. Williams, and P. M. Wood. 1981. Neuron-Schwann cell interaction in basal lamina formation. *Dev. Biol.* 92:449–460.
13. Cherry, R. J. 1979. Rotational and lateral diffusion of membrane proteins. *Biochem. Biophys. Acta.* 559:289–327.
14. Chow, I., and M.-M. Poo. 1982. Redistribution of cell surface receptors induced by cell-cell contact. *J. Cell Biol.* 95:510–518.
15. Coombs, J. S., J. C. Eccles, and P. Fatt. 1955. The electrical properties of the motoneurone membrane. *J. Physiol. (Lond.).* 130:291–325.
16. Damjanovich, S., L. Tron, J. Szollosi, R. Zidovetzki, W. L. Vaz, F. Regateiro, D. J. Arndt-Jovin, and T. M. Jovin. 1983. Distribution and mobility of murine histocompatibility H-$2k^k$ antigen in the cytoplasmic membrane. *Proc. Natl. Acad. Sci. USA.* 80:5985–5989.
17. Darbon, H., and K. J. Angelides. 1984. Structural mapping of the voltage-dependent sodium channel. *J. Biol. Chem.* 259:6074–6084.
18. Edidin, M., and M. Zuniga. 1984. Lateral diffusion of wild-type and mutant Ld Antigens in L cells. *J. Cell Biol.* 99:2333–2335.
19. Ellisman, M. H. 1979. Molecular specializations of the axon membrane at nodes of Ranvier are not dependent upon myelination. *J. Neurocytol.* 8:719–735.
20. Ellisman, M. H., and S. R. Levinson. 1982. Immunocytochemical localization of sodium channel distribution in the excitable membranes of *Electrophorus electricus. Proc. Natl. Acad. Sci. USA.* 79:6707–6711.
21. Ellisman, M. H., and K. R. Porter. 1980. Microtrabecular structure of the axoplasmic matrix, visualization of cross-linking structures, and their distribution. *J. Cell Biol.* 87:464–479.
22. Elmer, L. E., B. O'Brien, T. J. Nutter, and K. J. Angelides. 1985. Physicochemical characterization of the α-peptide of the sodium channel from rat brain. *Biochemistry.* 24:8128–8137.
23. Elson, E. L., and J. A. Reidler. 1979. Analysis of cell surface interactions by measurements of lateral mobility. *J. Supramol Struct.* 12:481–489.
24. Elson, E. L., and J. Schlessinger. 1979. Long-range motions on cell surfaces. *In* The Neurosciences. 4th Study Program. F. O. Schmitt and F. G. Worden, editors. The MIT Press, Cambridge, MA. 691–701.
25. Frank, E., and G. D. Fishbach. 1979. Early events in neuromuscular formation *in vitro. J. Cell Biol.* 83:143–158.
26. Hartshorne, R. P., and W. A. Catterall. 1984. The sodium channel from rat brain. Purification and subunit composition. *J. Biol. Chem.* 259: 1667–1695.
27. Henis, Y., and E. L. Elson. 1981. Inhibition of the mobility of mouse lymphocyte surface immunoglobulins by locally bound concanavalin A. *Proc. Natl. Acad. Sci. USA.* 78:1072–1076.
28. Jackson, M. B., H. Lecar, D. E. Brenneman, S. Fitzgerald, and P. G. Nelson. 1982. Electrical development in spinal cord cell culture. *J. Neurosci.* 2:1052–1061.
29. Klausner, R. D., A. M. Kleinfeld, R. L. Hoover, and M. J. Karnovsky. 1980. Lipid domains in membranes: evidence derived from structural perturbations induced by free fatty acids and lifetime heterogeneity analysis. *J. Biol. Chem.* 255:1286–1295.
30. Koppel, D. E., M. P. Sheetz, and M. Schindler. 1981. Matrix control of protein diffusion in biological membranes. *Proc. Natl. Acad. Sci. USA.* 78:3576–3580.
31. Kristol, C., C. Sandic, and K. Akert. 1978. Intramembranous particles of the nodes of Ranvier of the cat spinal cord: a morphometric study. *Brain Res.* 142:391–400.
32. Lander, A. D., D. K. Fujii, and L. F. Reichardt. 1985. Laminin is associated with the "neurite outgrowth-promoting factors" found in conditioned media. *Proc. Natl. Acad. Sci. USA.* 82:2183–2187.
33. Lazarides, E., W. J. Nelson, and T. Kasamatsu. 1984. Segregation of two spectrin forms in the chicken optic system: A mechanism for establishing restricted membrane-cytoskeletal domains in neurons. *Cell.* 36:269–278.
34. Levine, J., and M. Willard. 1981. Fodrin: axonally transported polypeptides associated with the internal periphery of many cells, *J. Cell Biol.* 90:631–643.
35. Linser, P. B., K. E. Smith, and K. J. Angelides. 1985. A comparative analysis of glial and neuronal markers in the retina of fish: variable character of horizontal cells. *J. Comp. Neuron.* 237:264–272.
36. Miller, J. A., W. S. Agnew, and S. R. Levinson. 1983. Principal glycoprotein of the tetrodotoxin/saxitoxin binding protein from *Electrophorus electricus*: isolation and partial chemical and physical characterization. *Biochemistry.* 22:462.
37. Myles, D. G., P. Primakoff, and D. E. Koppel. 1984. A localized surface protein of guinea pig sperm exhibits free diffusion in its domain. *J. Cell Biol.* 98:1905–1909.
38. Nigg, E. A., and R. J. Cherry. 1980. Achorage of a band 3 population at the erythrocyte cytoplasmic membrane surface: protein rotational diffusion measurements. *Proc. Natl. Acad. Sci. USA.* 77:4702–4706.
39. Poo, M. M. 1982. Rapid lateral diffusion of functional Ach receptors in embryonic muscle cell membrane. *Nature (Lond.).* 295:332–335.
40. Poo, M. M., and R. A. Cone. 1984. Lateral diffusion of rhodopsin in the photoreceptor membrane. *Nature (Lond.).* 247:438–441.
41. Porter, K. R., H. R. Byers, and M. H. Ellisman. 1979. The cytoskeleton. *In* The Neurosciences. 4th Study Program. F. O. Schmitt and F. G. Worden, editors. The MIT Press, Cambridge, MA. 703–722.
42. Ransom, B. R., E. Neale, M. Henkart, P. N. Bullock, and P. G. Nelson. 1977. Mouse spinal cord in cell culture. I. Morphology and intrinsic neuronal electrophysiologic properties. *J. Neurophysiol.* 40:1132–1150.
43. Ritchie, J. M., and R. B. Rogart. 1979. Density of sodium channels in mammalian myelinated nerve fibers and nature of the axonal membrane under the myelin sheath. *Proc. Natl. Acad. Sci. USA.* 74:211–215.
44. Rosenbluth, J. 1976. Intramembranous particle distribution at the node of Ranvier and adjacent axolemma in myelinated axons of the frog brain. *J. Neurocytol.* 5:731–745.
45. Saffman, P. G., and M. Delbruck. 1975. Brownian motion in biological membranes. *Proc. Natl. Acad. Sci. USA.* 72:3111–3113.
46. Schlessinger, J., and E. L. Elson. 1982. Fluorescence methods for studying membrane dynamics. *Methods Exp. Phys.* 20:197–227.
47. Scott, D., K. E. Smith, B. O'Brien, and K. J. Angelides. 1985. Characterization of mammalian neurofilament proteins: subunit stoichiometry and morphology of native and reconstituted filaments. *J. Biol. Chem.* 259: 10736–10747.
48. Shaw, G., and K. Weber. 1981. The distribution of the neurofilament triplet proteins within individual neurones. *Exp. Cell Res.* 136:119–125.
49. Small, R. K., and K. H. Pfenninger. 1983. Components of the plasma membrane of growing axons. I. Size and distribution of intramembrane particles. *J. Cell Biol.* 98:1422–1433.
50. Small, R. K., M. Blank, R. Ghez, and K. H. Pfenninger. 1984. Components of the plasma membrane of growing axons. II. Diffusion of membrane protein complexes. *J. Cell Biol.* 98:1434–1443.
51. Srinivasan, Y., L. Elmer, J. Q. Davis, V. Bennett, and K. J. Angelides. 1987. Control of sodium channel mobility in nerve: brain ankyrin and fodrin associate with voltage-dependent sodium channels. *Nature (Lond.).* In press.
52. Strichartz, G. R., R. K. Small, and K. H. Pfenninger. 1983. Components of the plasma membrane of growing axons. III. Saxitoxin binding to sodium channels. *J. Cell Biol.* 98:1444–1452.
53. Stuhmer, W. and W. Almers. 1982. Photobleaching through glass micropipettes: sodium channels without lateral mobility in the sarcolemma of frog skeletal muscle. *Proc. Natl. Acad. Sci. USA.* 79:946–950.
54. Tank, D. W., E. S. Wu, and W. W. Webb. 1982. Enhanced molecular diffusibility in muscle membrane blebs: release of lateral constraints. *J. Cell Biol.* 92:707–712.
55. Thompson, C. L., K. J. Angelides, J. L. Velasquez, and E. M. Barnes, Jr. 1987. Distribution, mobility, and function of benzodrazepine receptors on primary cultures of vertebrate neurons. *Adv. Biochem. Pharmacol.* In press.

56. Waechter, C., J. W. Schmidt, and W. A. Catterall. 1983. Glycosylation is required for maintenance of functional sodium channels in neuroblastoma cells. *J. Biol. Chem.* 258:5117–5123.
57. Waxman, S. G. 1981. Cytochemical heterogeneity of the axon membrane. *Trends Neurosci.* 4:7–9.
58. Wier, M. L., and M. Edidin. 1986. Effects of cell density and extracellular maxtix on the lateral diffusion of major histocompatibility antigens in cultured fibroblasts. *J. Cell Biol.* 103:215–222.
59. Wiley-Livingston, C. A., and M. H. Ellisman. 1980. Development of axonal membrane specializations defines nodes of Ranvier and precedes Schwann cell myelin elaboration. *Dev. Biol.* 79:334–355.
60. Wiley-Livingston, C. A., and M. H. Ellisman. 1980. Rows of dimeric particles within the axolemma and juxtaposed particles within glia, incorporated into a new model for the paranodal glial-axonal junction at the node of Ranvier. *J. Cell Biol.* 84:261–280.
61. Wolf, D. E., P. Henkart, and W. W. Webb. 1980. Diffusion patching, and capping of stearoylated dextrans on 3T3 cell plasma membranes. *Biochemistry.* 19:3893–3904.